bare space (~70% of total) (Fig. 3), allowing *Botrylloides* recruits that had survived beneath the *Molgula* "canopy" to expand. A similar pattern was observed among communities initially composed of only the semelparous colonial ascidian *Botryllus schlosseri* (*19*) (not shown), which died after reproducing. "Boom and bust" population cycles are characteristic of many epifaunal marine invertebrates (*17–20*), and this feature may contribute substantially to the susceptibility of these simple communities to invasion.

Species-rich communities appear to be buffered from such fluctuations in space availability. Although the abundance of each species in multispecies communities varied, these variations were out of phase, and the amount of open space that became available was less than that in simpler communities. For example, communities that initially contained *Botryllus*, *Molgula*, *Cryptosula*, and *Ciona* showed little change in the availability of free space throughout the course of the experiment (Fig. 3). This resulted from the sequential replacement of species; when one species declined, others increased and thus maintained high total cover. Because little space became available in these experiments, *Botrylloides* recruits had little room to grow, and few survived (Fig. 2). The consistently high cover in more species-rich communities may also reduce new recruitment of exotic invaders into these communities because these organisms typically do not settle directly on resident adults (*21*). In theory, a single species that could effectively monopolize space for a long period of time could resist invasion at least as well as a multispecies assemblage. However, the existence of such species in shallow-water epifaunal communities such as these appears unlikely because of the short life-span of most species, the absence of a rigid competitive hierarchy, and the importance of "priority" effects (*17*). Differences in primary space availability appear to drive the relation between diversity and invasibility in this system, but this model should be applicable to any system in which the limiting resources (such as light or nutrients) are clearly identifiable.

All native species used in our experiments could be placed in the same trophic and functional groupings, as they are all sessile, suspension-feeding invertebrates. As has been proposed for other communities (*22*), functionally redundant species may represent a form of biological insurance against the inevitable loss of any one species as a consequence of natural population cycles or disturbances. Our results lend empirical support to this idea from the marine environment, strengthening the argument for efforts to preserve naturally occurring biodiversity, regardless of whether some species are functionally similar. Because biodiversity loss promotes invasion and successful invasion may further decrease biodiversity (*2–4*), a negative feedback cycle may be initiated that ultimately results in severe impoverishment and homogenization of the global biota.

References and Notes

1. D. S. Wilcove, D. Rothstein, J. Dubow, A. Philips, E. Losos, *Bioscience* **48**, 607 (1998).
2. J. T. Carlton and J. B. Geller, *Science* **261**, 78 (1993).
3. J. T. Carlton, in *San Francisco Bay: The Urbanized Estuary*, T. J. Conomos, Ed. (California Academy of Sciences, San Francisco, 1979), pp. 427–444.
4. F. H. Nichols, J. K. Thompson, L. E. Schemel, *Mar. Ecol. Prog. Ser.* **66**, 95 (1990); J. Travis, *Science* **262**, 1366 (1993).
5. *Harmful Non-Indigenous Species in the United States* (Office of Technology Assessment, Washington, DC, 1993).
6. M. D. Fox and B. J. Fox, in *Ecology of Biological Invasions: An Australian Perspective*, R. H. Groves and J. J. Burdon, Eds. (Australian Academy of Sciences, Canberra, 1986), pp. 57–66.
7. M. B. Usher, *Biol. Conserv.* **44**, 119 (1988); A. N. Cohen and J. T. Carlton, *Science* **279**, 555 (1998).
8. C. S. Elton, *The Ecology of Invasions by Animals and Plants* (Methuen, London, 1958).
9. T. J. Case, *Proc. Natl. Acad. Sci. U.S.A.* **87**, 9610 (1990).
10. G. R. Robinson, J. F. Quinn, M. L. Stanton, *Ecology* **76**, 786 (1995); J. V. Robinson and J. E. Dickerson, *Oecologia* **61**, 169 (1984); S. L. Pimm, in *Biological Invasions: A Global Perspective*, J. A. Drake *et al.*, Eds. (Wiley, New York, 1989), pp. 351–367; D. Simberloff, in *Ecology of Biological Invasions of North America and Hawaii*, H. A. Mooney and J. A. Drake, Eds. (Springer-Verlag, New York, 1986), pp. 3–26.
11. A. Planty-Tabacchi, E. Tabacchi, R. J. Naiman, C. Deferrari, H. Decamps, *Conserv. Biol.* **10**, 598 (1996); S. K. Wiser, R. B. Allen, P. W. Clinton, K. H. Platt, *Ecology* **79**, 2071 (1998); T. J. Stohlgren *et al.*, *Ecol. Monogr.* **69**, 47 (1999).
12. J. McGrady-Steed, P. M. Haris, P. J. Morin, *Nature* **390**, 162 (1997); D. Tilman, *Ecology* **78**, 81 (1997); J. M. H. Knops *et al. Ecol. Lett.* **2**, 286 (1999).
13. J. Carlton, *Conserv. Biol.* **3**, 265 (1989); J. Berman, L. Harris, W. Lambert, M. Buttrick, M. Dufresne, *Conserv. Biol.* **6**, 432 (1992).
14. R. W. Osman and R. B. Whitlatch, *Mar. Ecol. Prog. Ser.* **117**, 111 (1995).
15. Experimental communities were suspended from floating docks so that they were 1.0 m beneath the water surface. The docks naturally support a lush growth of epifaunal invertebrates dominated by the species used in the experiments.
16. P. K. Dayton, *Ecol. Monogr.* **41**, 351 (1971).
17. J. P. Sutherland and R. H. Karlson, *Ecol. Monogr.* **47**, 425 (1977); L. W. Buss and J. B. C. Jackson, *Am. Nat.* **113**, 223 (1979).
18. R. W. Osman, *Ecol. Monogr.* **47**, 37 (1977).
19. R. K. Grosberg, *Evolution* **42**, 900 (1988).
20. K. D. McDougall, *Ecol. Monogr.* **13**, 321 (1943).
21. R. W. Osman and R. B. Whitlatch, *J. Exp. Mar. Biol. Ecol.* **190**, 199 (1995).
22. S. Naeem and S. Li, *Nature* **390**, 507 (1997); D. Tilman *et al.*, *Science* **277**, 1300 (1997); D. Tilman and J. A. Downing, *Nature* **367**, 363 (1994).

23. We thank M. Berger, H. Lisitano, E. Rogers, and S. Smith for assistance conducting these experiments and the Jesse B. Cox Charitable Trust and NSF for providing funding for our work. A. Lohrer, P. Renaud, and two anonymous reviewers provided helpful comments on earlier drafts of the manuscript.

29 June 1999; accepted 11 October 1999

Structural Analysis of the Mechanism of Adenovirus Binding to Its Human Cellular Receptor, CAR

Maria C. Bewley, Karen Springer, Yian-Biao Zhang, Paul Freimuth,* John M. Flanagan*

Binding of virus particles to specific host cell surface receptors is known to be an obligatory step in infection even though the molecular basis for these interactions is not well characterized. The crystal structure of the adenovirus fiber knob domain in complex with domain I of its human cellular receptor, coxsackie and adenovirus receptor (CAR), is presented here. Surface-exposed loops on knob contact one face of CAR, forming a high-affinity complex. Topology mismatches between interacting surfaces create interfacial solvent-filled cavities and channels that may be targets for antiviral drug therapy. The structure identifies key determinants of binding specificity, which may suggest ways to modify the tropism of adenovirus-based gene therapy vectors.

Many viral infections are initiated by the specific binding of specialized proteins or attachment factors on the virion's surface to glycoprotein receptors on the surface of host cells. Enveloped viruses, such as human immunodeficiency virus (HIV), attach to host cells by means of spike-like membrane glycoproteins, whereas most nonenveloped viruses, such as poliovirus, attach by means of specialized domains integral to their capsids. Adenoviruses (Ad) are hybrids: They are nonenveloped but have trimeric fibers (320 to 587 residues) emanating from the vertices of their icosahedral capsid, which terminate in

Biology Department, Brookhaven National Laboratory, Upton, NY 11973, USA.

*To whom correspondence should be addressed. E-mail: flanagan@bnlbio.bio.bnl.gov and Freimuth@bnl.gov

globular knob domains (~175 residues). Infection is initiated by the formation of a high-affinity complex between these knob domains and a host cell surface protein. For the majority of the >50 known Ad serotypes, this receptor is CAR, which is also the cellular receptor for group B coxsackieviruses (*1*). CAR is an integral membrane protein of unknown cellular function that is expressed in a wide range of human and murine cell types. Its two extracellular immunoglobulin superfamily (Ig) domains mediate Ad and coxsackievirus B infections, possibly with different parts of the molecule. After CAR binding, Ad replicates within the nuclei of cells, causing frequent and generally mild infections of the upper respiratory and gastrointestinal tracts. Their efficiency of infection and their ability to transport large amounts of DNA are two of the properties of Ad that have prompted their development as gene delivery vectors for experimental gene therapy (*2*). Understanding the molecular details of the knob-CAR complex is one step toward developing better gene-delivery systems with altered tropism or increased receptor binding affinity, or both.

The knob domain from Ad serotype 12 (Ad12) and the NH_2-terminal domain of human CAR (CAR D1) were overexpressed in *Escherichia coli* as soluble protein fragments. To determine the molecular basis for the specificity and tight affinity of this interaction (*3*), we crystallized and determined the structure of the Ad12 knob alone and in complex with human CAR D1 to 2.6 Å resolution (*4*). The data collection and refinement statistics are shown in Table 1. Adopting the nomenclature of Xia, used for the structure of the Ad5 knob (*5*), Ad12 knob momomers also have an eight-stranded antiparallel β-sandwich fold. The packing of strands J, C, B, and A (called a sheet) from adjacent monomers form the tightly packed trimer interface and create a large cavity located along the central threefold axis of symmetry that was proposed as a potential receptor binding site (*5*). Strands G, H, D, and I (R sheet) form a solvent-exposed β sheet that was also identified as a putative receptor-binding site (*5*). The major difference between the structures of the two knobs, which both bind CAR, is in the HI loop, which in Ad12 (residues 548 to 556) is well ordered but in Ad5 (residues 536 to 549) is a five-residue extended and disordered loop (*6*).

To locate the actual CAR-binding site on Ad12 knob, we solved the structure of the Ad12 knob–human CAR D1 complex (Table 1). It has a triskelion shape with three CAR D1 monomers bound per knob trimer (Fig. 1A). This multiplicity for CAR binding coupled with the high affinity of the interaction may contribute to the high efficiency of Ad infection. In the complex, CAR D1 (residues 1 to 123 of the mature protein) adopts a β-sandwich fold that is characteristic of Ig variable (Igv) domains (Fig. 1B). CAR D1 does not bind at either of the predicted sites on knob. Instead, each CAR D1 molecule binds at the interface between two adjacent Ad12 knob monomers, consistent with the observation that most neutralizing antibodies to knob are directed against the trimer, rather than the monomer (*7*). In contrast to some viruses, which undergo a conformational change to expose the binding site, we find that complex formation in Ad occurs without any notable rearrangement in the knob structure. This may also be true of CAR D1, because in the complex it is structurally homologous to the unliganded forms of CD4 and the myelin adhesion molecule (*8*). Compatible with the role of CAR D1 in attaching adenovirus to the cell membrane, its COOH-terminus lies 180° away from the NH_2-terminal end of the knob trimer and hence the viral fiber axis. Although the current model does not provide direct information concerning the orientation of CAR D2 (residues 126 to 222) relative to D1, comparisons of CAR D1 with structures of homologous proteins, solved with both D1 and D2 domains, suggest that CAR D2 does not make extensive contacts with knob (*9*). This is consistent with the observation that soluble CAR D1 alone is sufficient for knob binding and is an inhibitor of viral infection for cells in culture (*3*).

The nature of the specificity of Ad12 knob for CAR is suggested by the structure of the complex, particularly at the interface that is formed by four loop regions of Ad12 knob interacting with a single face of the CAR D1 sandwich. Specifically, the AB loop, the carboxyl ends of the DE loop, and the very short F strand of one knob monomer and the FG loop of the adjacent knob monomer interact with strands C, C′, C″, and the second half of strand F in CAR D1. The AB loop (colored yellow in Fig. 1A) contributes over 50% of interfacial protein-protein interactions, including the three hydrogen bonds involving conserved atoms in Ad12 knob [D415 O on knob forms a hydrogen bond with K104 Nζ on CAR D1 (D415 O/K104 Nζ), L426 O/Y64 OH, and K429 Nζ/E37 Oε2] (*10*), and thus may be the key anchor for the complex. This loop spans the width of the CAR D1, held at one end by D415 and at the other end by E425, which changes rotomer conformation upon CAR D1 binding to accommodate the approaching side chain of Y61. In the middle of the AB loop, the conserved residue P418 makes contacts with residues E37, V51, and L54 in CAR D1. Substitution of L54 with alanine in CAR D1 completely abrogates CAR binding, which is consistent with a role for these interactions in complex stability. The importance of the AB loop is further emphasized when comparing the sequence of non–CAR-binding Ad serotypes such as subgroup B (serotypes 3 and 7), which have evolved to bind a different receptor (*11*), or serotypes 40 and 41, where two types of fiber exist on the same virus but only one fiber type binds CAR (*12*) (Fig. 1C). The sequenc-

Table 1. Summary of data collection statistics. Numbers in parentheses refer to data in the outermost resolution shell. AU, asymmetric unit. I, intensity. R_{free} is based on ~3% of the data.

	Ad12 knob	Ad12 knob–CAR D1	Thimerosal
Crystal parameters			
Space group	$P2_1$	$P4_332$	$P4_332$
Cell dimensions (Å)	a = 61.91, b = 104.82	a = 167.85	a = 167.44
Matthew's coefficient	2.12	5.67	5.63
No. of molecules in AU	2 knob trimers	1 knob monomer 1 CAR D1	1 knob monomer 1 CAR D1
Data collection			
Resolution (Å)	30–2.6	30–2.6	30–3.4
Unique observations	27987	24636	11487
Redundancy	2.5	14.2	13.8
R_{merge} (%)*	10.0 (22.4)	7.0 (34.6)	9.8 (23.6)
Completeness (%)	100.0 (100)	100.0 (100)	99.6 (99.7)
$I/\sigma I$	10 (3)	20 (6)	12 (5)
Phasing power, FOM			1.1, 0.2
Refinement statistics			
Resolution limits (Å)	20–2.6	20–2.6	
No. of protein atoms	8406	2342	
No. of water molecules	0	70	
R factor (%)†	24.1	22.5	
R_{free} (%)	29.4	24.9	
No. of reflections in free set	1125	739	
Geometric parameters			
Bond length (Å)	0.008	0.008	
Bond angle (°)	1.70	1.65	

*$R_{merge} = \Sigma_h \|I_{obs}\| - |I_{avg}\| / \Sigma |I_{avg}|$. †$R = \Sigma_h \|F_P\| - |F_M\| / \Sigma |F_P|$, where $|F_P|$ is the structure factor of observed data and $|F_M|$ is the structure factor of the model.

es in this region of the non–CAR-binding serotypes diverge widely from each other and from known CAR-binding serotypes. Specifically, the knob domains of non–CAR-binding fibers either have insertions or deletions in this loop relative to the conserved residues, P418 and N419.

To further explore the idea that the AB loop is important in CAR binding, we constructed a number of knob variants that mimic non–CAR-binding knobs in this region. The double substitution P417E and P418A, which converts the Ad12 AB loop to a sequence similar to Ad3, the insertion of TI before S421, which lengthens the AB loop, and the deletion of E425 and L426, which shortens the AB loop, all abrogate CAR D1 binding (*13*). In addition, we made single amino acid substitutions outside this loop, the majority of which behaved in a manner that is consistent with the structure we constructed (*14*). The results are consistent with the hypothesis that the AB loop is a primary determinant for the specificity of most Ad serotypes for CAR. Unexpectedly, the deletions of G550 and I551 in the HI loop significantly reduced the affinity of CAR D1 binding even though the residues do not interact directly with the receptor or model. In the native structure, there are water-mediated hydrogen bonds between G550N and G550O in the HI loop and R518O and A521N in the FG loop that stabilize the FG loop in a conformation through which it can make direct contacts with CAR D1. Thus, a likely explanation for the decreased affinity of Ad12 for CAR D1 when G550 and I551 are deleted is that the loss of these hydrogen bonds, because of the removal of G550, allows the FG loop more flexibility in conformation. Although this result highlights the limitations of using a purely mutational strategy for identifying knob's receptor-binding sites, it shows that altering the amino acid sequence in the AB loop may be one way of changing the tropism of Ad-based gene therapy vectors.

In protein-protein complexes, the interacting surfaces are typically well conserved and usually display a high degree of surface complementarity. The CAR D1 binding site in Ad12 knob lies along a ridge of residues primarily from the AB loop that are generally highly conserved, although some sequence variability is seen (*14*). It is located on the side of the molecule at the interface between adjacent monomers (Fig. 2A). In total, the complex formation buries ~1880 Å^2 of mixed hydrophobic and hydrophilic surfaces at each knob-CAR interface: 960 Å^2 of surface are contributed by knob (820 Å^2 from one monomer and 140 Å^2 from the second monomer) and 920 Å^2 by CAR D1 (Fig. 2, B and C) (*15*). These values are within the range typically observed for protein-protein interactions. However, the interface is atypical because the Ad12 knob and

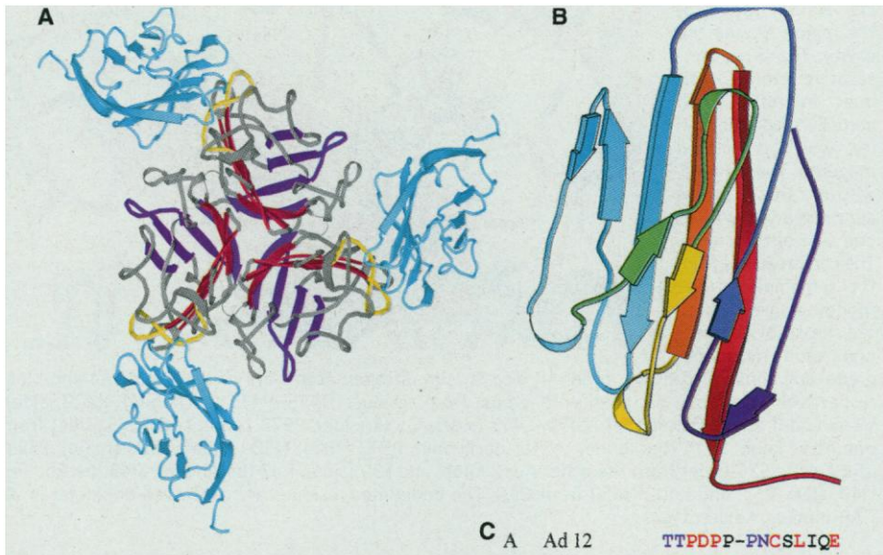

Fig. 1. The Ad12 knob–CAR D1 complex and the importance of the AB loop. (**A**) Ribbon diagram of the Ad12 knob–CAR D1 complex viewed down the viral fiber. The core of each knob monomer comprises an eight-stranded antiparallel β sandwich, although about 65% of the residues are found in ordered surface exposed loops and turns. The V sheet is colored purple and the R sheet and HI loop are colored magenta. The AB loop is highlighted in yellow, and all other regions are gray. About 2050 Å^2 of primarily hydrophobic surface per monomer is buried upon trimerization of the knob domains. In Ad12 knob, the interfacial residues are D415, P417, P418, I426 (AB loop), V450, K451 (CD loop), and Q487, Q494, S497, and V498 (E and F strands) from one monomer, and P517, P519, N520, and E523 (FG loop) from the other. (**B**) Ribbon diagram of the CAR D1 domain from the complex colored in a rainbow from blue to red. Strands in the foreground are D, E, B, and A, and strands in the background are C″, C′, C, F, and G from left to right, respectively. In CAR D1, the interfacial residues are P33, E37, L39, V48, D49, V51, L54, S56, Y61, D62, E63, Y64 (strands C, C′, and C″), K102, K104, A106, and P107 (later half of F). This figure was generated in MOLSCRIPT (*29*). (**C**) Amino acid sequence alignment of residues in the AB loop for all knob subgroups. Adenovirus subgroups A, C, D, E, and the long fiber of F bind CAR, whereas subgroup B and short fiber knobs of F do not. Residues conserved in CAR-binding serotypes are colored blue, those with 1 amino acid different are colored in red, and all other residues are colored in black. On a wider alignment, with the use of all available adenovirus sequences, the pattern of conservation of proline and aspartate was unchanged (*14*).

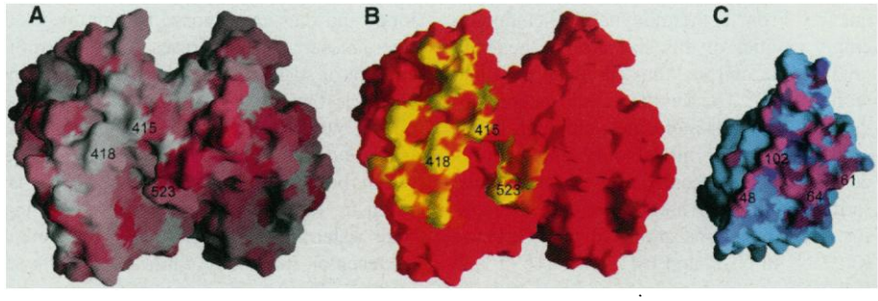

Fig. 2. A molecular surface representation of the interface in the Ad12 knob-CAR D1 complex. (**A**) Sequence conservation surface diagram of two knob monomers viewed at the CAR interface. The molecules are colored on a sliding scale from white (conserved) to red (nonconserved). Conservation analysis was based on an alignment of all human Ad knob sequences available in GenBank. A white strip of conservation transects the surface of the molecule. Upon binding, the CAR D1 molecule occludes the conserved strip on Ad12 knob. (**B**) Surface diagram of two adjacent Ad12 knob monomers shown in the same view as (A). The molecules are colored on a sliding scale from yellow (contact) to red (no contact). Atoms in contact with CAR D1 are shared between monomers. (**C**) Surface diagram of CAR D1. The molecules are colored on a sliding scale from magenta (contact) to cyan (no contact). This figure was generated with GRASP (*30*).

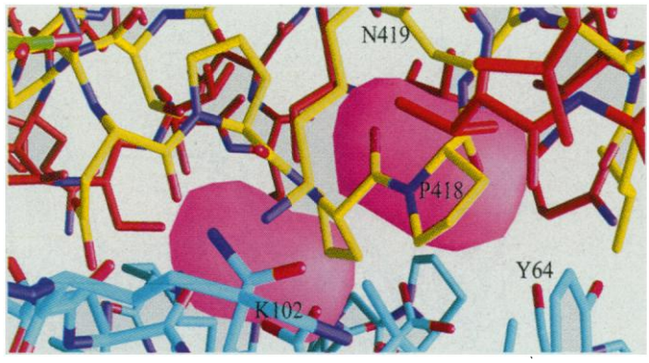

Fig. 3. CPK model of the region around the cavity. The three consecutive proline residues in Ad12 knob partially shape the cavity, which is colored magenta. The AB loop, whose carbon atoms are colored yellow, lines one side of the cavity. The carbon atoms from the remainder of the monomer are colored red, those of the second knob monomer, green, and those of CAR D1, cyan. All oxygen and nitrogen atoms are colored light red and blue, respectively. The cavity is lined with atoms from residues D415, P416 (backbone), K429 (side), V448 (side), G449 (backbone), V450, L455 (side), Q535 (side), P573 (side), and S575 (side) from one Ad12 knob; S514 (backbone), A515 (backbone), P517 (side), N520 (side), A524 (main), E523, K525, and S526 (side) from the other Ad12 knob; and L39 (side), K47 (backbone), V48 (backbone), D49, Q50, V51, and K102 (side) from CAR. The underlined residues are conserved or similar in all CAR-binding Ad serotypes.

CAR D1 residues each produce a surface that, when united with its partner, creates a prominent channel and two adjacent cavities. A consequence of this discontinuous interface is that the actual footprints of the interacting surfaces in the complex are ~15% larger than would be predicted from the values of buried surface area.

The high affinity of the knob-CAR D1 complex directly conflicts the general observation that shape mismatches in the interface of protein complexes tend to correlate with low-affinity binding (*16*). In the Ad12 knob–CAR D1 complex, the lack of van der Waals interactions between the protein surfaces may be partially compensated for by solvent molecules within the cavities and interfacial channel (Fig. 3A). The two equally sized (total volume ~120 Å^3) cavities are separated by P418 in the AB loop of Ad12 knob interacting with residues in CAR D1, and the cavities are lined with a mixture of hydrophobic and polar groups, >60% of which either are backbone atoms or are conserved in sequence. From a thermodynamic standpoint, empty cavities of this size are energetically unfavorable and are thus likely to be filled with solvent. The cavities could accommodate ~four water molecules, although in the current structural model only one well-ordered water molecule was observed that formed a bridging interaction with the conserved or backbone atoms of E37 Oε1 and K102 Nζ in CAR and D415 O, P416 O, and K429 Nζ in Ad12 knob. In addition, there is a solvent-lined interfacial channel, created by the packing of residues N415, K429, V450, L455, N520, S522, and E523 in Ad12 knob (Fig. 2C) against residues V48, N49, K102, V51, Y64, and P66 in CAR D1 (Fig. 2D). In the current model, four ordered water molecules markedly increase the interfacial contact surface and may thus act as molecular glue. Weaker electron density, also observed throughout the cavities and channel, may be indicative of additional mobile water molecules. The identification of the key residues involved in the Ad12 knob–CAR D1 interface may aid in the design of Ad-based gene targeting vectors that no longer bind CAR but specifically target other cell surface receptors at a second site.

The results presented here, and those of others, suggest that viruses have developed at least two structural means of successfully binding their receptors. The receptor-binding sites in picornoviruses, such as poliovirus, and, by extension, the CAR-binding site on coxsackievirus B, are located in deep crevices or canyons on the capsid surface (*17, 18*). Burying the receptor-binding site in this way may act as an antigenic shield for the conserved residues that define receptor-binding specificity (*19*). By contrast, the structures and biochemical studies of the structurally unrelated Ad12 knob and the HIV gp120 in complex with their receptors (*20, 21*) show that their receptor-binding faces are surface loops and thus are exposed to immunoselective pressure. Both viruses bury a similar amount of surface area to create cavities and channels that may serve a dual purpose as both a water buffer and as molecular glue, because they mediate hydrogen bonds between backbone and conserved atoms. By using a noncomplementary interface that traps water molecules, the virus can maintain its receptor specificity while altering its sequence. Because this type of interface has been observed in two very different viruses, the water-buffer hypothesis may represent a second general mechanism by which viruses can successfully achieve the first stage of infection.

References and Notes

1. J. M. Bergelson *et al.*, *Science* **275**, 1320 (1997).
2. G. J. Nabel, *Proc. Natl. Acad. Sci. U.S.A.* **96**, 324 (1999).
3. P. Freimuth *et al.*, *J. Virol.* **73**, 1392 (1999).
4. The knob fiber protein (Ad12 knob) and the NH_2-terminal fragment (residues 22 to 125) of the cellular receptor (CAR D1) were expressed in *E. coli* and purified as described previously (*3*). Purified proteins were proteolysed separately with trypsin (10 mg/ml). The 1:3 (trimeric knob: CAR D1) complex was formed at room temperature and purified by anion exchange chromatography. Crystals of Ad12 knob were grown at room temperature with the sitting drop vapor diffusion method from an Ad12 knob solution of 20 mg/ml suspended over a reservoir of 26% polyethylene glycol (PEG) 3350. Showers of small, poorly ordered crystals grew over the course of a week and were used to seed a 10-μl drop containing equal volumes of Ad12 knob and 26% PEG 3350 over a reservoir of 26% PEG 3350. Typically, crystals grew overnight as rhombohedral plates (0.5 mm by 0.5 mm by 0.2 mm). They were flash cooled at 99 K with 50% PEG 3350 as a cryoprotectant. Crystals of the complex were grown at room temperature with the sitting drop vapor diffusion method from 0.9 M ammonium sulfate in 100 mM MES (pH 6.2). Mercury was introduced into the Ad12 knob–CAR D1 complex by soaking a single CAR D1-knob complex crystal in 10 mM thimerosal for 6 hours. Crystals were flash cooled at 99 K, with 50% ethylene glycol as a cryoprotectant. Data were processed with the HKL Program Suite (*22*). The structure of Ad12 knob was solved by molecular replacement (*23*), with a monomer of Ad5 knob [Protein Data Bank (PDB) accession number 1KNB.PDB] as a search model. Six monomers were placed and their positions were refined with rigid body refinement. Simulated annealing protocols in CNS (*24*) with the use of tight NCS restraints were punctuated by rounds of model building. The refinement statistics are shown in Table 1. The structure of the Ad12 knob–CAR D1 complex was determined with a combination of single isomorphous replacement (SIR), solvent flattening, and molecular replacement. The refined structure of the Ad12 knob monomer was used as a search model in molecular replacement. A single, clear solution was found corresponding to a monomer in the asymmetric unit such that the biological three-fold axis was coincident with the crystallographic axis. The heavy atom position was determined by visual inspection of a difference map with model phases, and its position was refined with MLPHARE (*23*). Phase combination with the use of the Ad12 knob structure and the experimental SIR phases followed by solvent flattening with the program DM (*23*) resulted in a map with a mean figure of merit (FOM) of 0.74. The structure was refined with CNS punctuated by rounds of model building.
5. D. Xia, L. J. Henry, R. D. Gerard, J. Deisenhofer, *Structure* **2**, 1259 (1994).
6. Ad12 knob is 48% identical and 78% similar in sequence to Ad5 knob, which also binds CAR. The structures are essentially identical and have a root mean square deviation of 1.2 Å when equivalent Cα atoms are superimposed.
7. P. Fender, A. H. Kidd, R. Brebant, M. E. C. Oeberg, J. Drouet, *Virology* **214**, 110 (1995); L. J. Henry, D. Xia, M. E. Wilke, J. Deisenhofer, and R. D. Gerard, *J. Virol.* **68**, 5239 (1994).
8. On the basis of an search of the DALI database (*25*), the structure of CAR D1 most closely resembles the structures of (in descending order) the extracellular domain of the myelin adhesion molecule (*26*), domain 1 of human CD4 (*27*), a receptor for HIV, and several other cell surface glycoproteins. Although all of these molecules share a common fold, large differences in strand lengths and loop conformations are evident when equivalent atoms are superimposed.
9. Domain 1 of CD4 (1cdh.pdb), ICAM-1 (1iam.pdb and lic1.pdb), and ICAM2 (1zxq.pdb) (where the names of the molecules are followed by their PDB access identification numbers) were superimposed on the structure of CAR D1. The positions of the second domain were used to infer a possible position of CAR D2.
10. Single-letter abbreviations for the amino acid residues are as follows: A, Ala; C, Cys; D, Asp; E, Glu; F,

Phe; G, Gly; H, His; I, Ile; K, Lys; L, Leu; M, Met; N, Asn; P, Pro; Q, Gln; R, Arg; S, Ser; T, Thr; V, Val; W, Trp; and Y, Tyr.
11. P. W. Roelvink *et al.*, *J. Virol.* **72**, 7909 (1998).
12. H. Y. Yeh, N. Pieniazek, D. Pieniazek, H. Gelderblom, R. B. Luftig, *Virus Res.* **33**, 179 (1994).
13. All Ad12 knob variants listed were constructed by primer-directed PCR mutagenesis and confirmed by nucleotide sequence analysis. The knob variants were purified as previously described for native Ad12 knob. A filter-binding assay was used as an initial screen for the effects of substitutions in knob on CAR D1 binding. Purified variant or wild-type His-tagged knob proteins were briefly immobilized on nitrocellulose membranes (5 μg per dot) and fixed with 0.25% glutaraldehyde in phosphate-buffered saline (PBS). The membranes were probed with biotinylated CAR D1 (5 mg/ml), and bound CAR D1 was visualized with 1:500 horseradish peroxidase (HRP)–conjugated mouse monoclonal antibody to biotin (Sigma) with the use of a chemiluminescent substrate (SuperSignal, Pierce, Rockford, IL). A duplicate membrane was used to quantitate bound protein with rabbit antiserum to Ad12 knob followed by HRP goat antibody to rabbit IgG (Cappel, Cochranville, PA) and chemiluminescent detection. All assays were performed in duplicate. Two other methods were used to confirm results and provide a more quantitative estimate for the effect of these substitutions. First, CAR D1 binding by knob variants were characterized by size exclusion chromatography (SEC) on a TSK G3000 SWXL (7.8 mm by 30 cm) column. The extent of complex formation in 25 mM MES (pH 6.5) and 200 mN NaCl was estimated from the changes in elution volume of the complex. Under these conditions, wild-type complex is well resolved from free CAR D1 and Ad12 knob (*3*). Second, we examined complex formation with a native polyacrylamide gel electrophoresis gel assay. Complexes formed at varying ratios of CAR D1 to Ad12 knob or its variants were electrophoresed on a 7% native gel. Under these conditions, free knob barely enters the gel, and the complex migrates between free knob and free CAR D1.
14. Supplemental data available at www.sciencemag.org/feature/data/1043056.shl.
15. Surface accessible areas were determined by the method of Lee and Richards (*28*) with the program ACCESS with a probe radius of 1.4 Å.
16. S. Ikemizu *et al.*, *Proc. Natl. Acad. Sci. U.S.A.* **96**, 4289 (1999).
17. J. K. Muckelbauer *et al.*, *Structure* **3**, 653 (1995).
18. J. Bella, P. R. Kolatkar, C. W. Marlor, J. M. R. Greve, M. G. Rossmann, *Proc. Natl. Acad. Sci. U.S.A.* **95**, 4140 (1998).
19. M. G. Rossmann, *J. Biol. Chem.* **264**, 14587 (1989).
20. P. D. Kwong *et al.*, *Nature* **393**, 648 (1998).
21. R. Wyatt *et al.*, *Nature* **393**, 705 (1998).
22. Z. Otwinowski and W. Minor, in *Methods in Enzymology*, vol. 276, C. W. Carter and R. M. Sweet, Eds. (Academic Press, New York, 1997), pp. 307–326.
23. CCP4, *The SRC(UK) Collaborative Computing Project No. 4: A Suite of Programs for Protein Crystallography* (Daresbury Lab, Warrington, UK, 1991).
24. A. T. Brunger *et al.*, *Acta Crystallogr. Sect. D Biol. Crystallogr.* **54**, 905 (1998).
25. L. Holm and C. Sander, *Science* **273**, 595 (1996).
26. L. Shapiro, J. P. Doyle, P. Hensley, D. R. Colman, W. A. Hendrickson, *Neuron* **17**, 435 (1996).
27. S. E. Ryu, A. Truneh, R. W. Sweet, W. A. Hendrickson, *Structure* **2**, 59 (1994).
28. B. Lee and F. M. Richards, *J. Mol. Biol.* **55**, 379 (1971).
29. P. J. Kraulis, *J. Appl. Crystallogr.* **24**, 946 (1991).
30. A. Nicholls, K. A. Sharp, B. Honig, *Proteins* **11**, 281 (1991).
31. The authors thank V. Graziano for analyzing the binding affinities of the knob variants; M. Rossmann, D. Engelman, C. Anderson, J. Dunn, and J. Kuryian for critically reading the manuscript and suggesting improvements; and L. Berman, R. Sweet, and J. Berendsen for access to beamlines X25, X12C, and X8C, respectively. This research was supported by NIH grant AI36251 to P.F. and by the Office of Biological and Environmental Research of the U.S. Department of Energy under Prime Contract DE-AC02-98CH10886 with Brookhaven National Laboratory. The macromolecular crystallography beamlines X25, X12C, and X8C, at the National Synchrotron Light Source, are also supported by NSF and by NIH grant 1P41 RR12408-01A1. Coordinates have been deposited in the Protein Data Bank with accession codes 1NOB and 1KAC for Ad12 knob and Ad12 knob in complex with CAR D1, respectively.

28 June 1999; accepted 30 September 1999

Regulation of Myosin Phosphatase by a Specific Interaction with cGMP-Dependent Protein Kinase Iα

Howard K. Surks,[1] Naoki Mochizuki,[1,2] Yasuyo Kasai,[1] Serban P. Georgescu,[1] K. Mary Tang,[1] Masaaki Ito,[3] Thomas M. Lincoln,[4] Michael E. Mendelsohn[1]*

Contraction and relaxation of smooth muscle are regulated by myosin light-chain kinase and myosin phosphatase through phosphorylation and dephosphorylation of myosin light chains. Cyclic guanosine monophosphate (cGMP)–dependent protein kinase Iα (cGKIα) mediates physiologic relaxation of vascular smooth muscle in response to nitric oxide and cGMP. It is shown here that cGKIα is targeted to the smooth muscle cell contractile apparatus by a leucine zipper interaction with the myosin-binding subunit (MBS) of myosin phosphatase. Uncoupling of the cGKIα-MBS interaction prevents cGMP-dependent dephosphorylation of myosin light chain, demonstrating that this interaction is essential to the regulation of vascular smooth muscle cell tone.

Smooth muscle cells are critical to the normal physiology of many of the organs of the body. Smooth muscle cells are the principal component of blood vessels, where they regulate vascular tone and play a central role in the pathogenesis of atherosclerosis and vascular diseases. Smooth muscle contraction and relaxation are regulated by the rise and fall of intracellular calcium levels (*1, 2*). An increase in intracellular calcium causes smooth muscle cell contraction by activation of the calcium/calmodulin-dependent myosin light-chain kinase, which phosphorylates myosin light chain and activates the contractile myosin adenosine triphosphatase (ATPase). A decrease in intracellular calcium causes inactivation of myosin light-chain kinase, accompanied by dephosphorylation of myosin light chain by the myosin light-chain phosphatase, PP1M (*2*). PP1M is a trimer comprising a 130-kD regulatory myosin-binding subunit (MBS), a 37-kD catalytic subunit (PP1c), and a 20-kD protein of uncertain function (M20) (*3*).

In smooth muscle, the sensitivity of the contractile apparatus to calcium is modulated by intracellular messengers that alter PP1M activity. Contractile agonists acting through signaling molecules such as protein kinase C, arachidonic acid, and rho kinase increase the sensitivity of vascular smooth muscle cells to contractile stimuli by inhibiting PP1M (*4*). Conversely, endogenous nitric oxide and related nitrovasodilators regulate blood pressure by activation of soluble guanylate cyclase, elevation of cGMP, and activation of cGMP-dependent protein kinase Iα (cGKIα), which is required for nitric oxide–mediated vasodilatation and leads to vasorelaxation by an unknown mechanism (*5*). Cyclic GMP–mediated vascular smooth muscle cell relaxation is characterized by both a reduction of intracellular calcium concentration and by activation of PP1M, which reduces the sensitivity of the contractile apparatus to intracellular calcium (*5, 6*). The mechanism by which cGMP increases PP1M activity and myosin light-chain dephosphorylation is unknown.

Kinases and phosphatases are targeted to subcellular locations by binding to specific targeting proteins that restrict the subcellular locale of these signaling enzymes (*7*). Anchoring proteins, such as the A-kinase anchoring pro-

[1]Molecular Cardiology Research Institute and Cardiology Division, Department of Medicine, Tufts University School of Medicine and New England Medical Center, Boston, MA 02111, USA. [2]Department of Pathology, Research Institute, International Medical Center of Japan, Tokyo 162-8655, Japan. [3]First Department of Internal Medicine, Mie University School of Medicine, Tsu 514, Japan. [4]Department of Pathology, Division of Molecular and Cellular Pathology, University of Alabama, Birmingham, AL 35294–0019, USA.

*To whom correspondence should be addressed. E-mail: mmendelsohn@lifespan.org

References and Notes

[1] **Isolation of a Common Receptor for Coxsackie B Viruses and Adenoviruses 2 and 5**

Jeffrey M. Bergelson; Jennifer A. Cunningham; Gustavo Droguett; Evelyn A. Kurt-Jones; Anita Krithivas; Jeong S. Hong; Marshall S. Horwitz; Richard L. Crowell; Robert W. Finberg

Science, New Series, Vol. 275, No. 5304. (Feb. 28, 1997), pp. 1320-1323.

Stable URL:

http://links.jstor.org/sici?sici=0036-8075%2819970228%293%3A275%3A5304%3C1320%3AIOACRF%3E2.0.CO%3B2-I

[2] **Development of Optimized Vectors for Gene Therapy**

Gary J. Nabel

Proceedings of the National Academy of Sciences of the United States of America, Vol. 96, No. 2. (Jan. 19, 1999), pp. 324-326.

Stable URL:

http://links.jstor.org/sici?sici=0027-8424%2819990119%2996%3A2%3C324%3ADOOVFG%3E2.0.CO%3B2-4

[16] **Crystal Structure of the CD2-Binding Domain of CD58 (Lymphocyte Function-Associated Antigen 3) at 1.8- angstrom Resolution**

Shinji Ikemizu; Lisa M. Sparks; P. Anton van der Merwe; Karl Harlos; David I. Stuart; E. Yvonne Jones; Simon J. Davis

Proceedings of the National Academy of Sciences of the United States of America, Vol. 96, No. 8. (Apr. 13, 1999), pp. 4289-4294.

Stable URL:

http://links.jstor.org/sici?sici=0027-8424%2819990413%2996%3A8%3C4289%3ACSOTCD%3E2.0.CO%3B2-A

LINKED CITATIONS

[18] **The Structure of the Two Amino-Terminal Domains of Human ICAM-1 Suggests How it Functions as a Rhinovirus Receptor and as an LFA-1 Integrin Ligand**

Jordi Bella; Prasanna R. Kolatkar; Christopher W. Marlor; Jeffrey M. Greve; Michael G. Rossmann

Proceedings of the National Academy of Sciences of the United States of America, Vol. 95, No. 8. (Apr. 14, 1998), pp. 4140-4145.

Stable URL:

http://links.jstor.org/sici?sici=0027-8424%2819980414%2995%3A8%3C4140%3ATSOTTA%3E2.0.CO%3B2-A

[25] **Mapping the Protein Universe**

Liisa Holm; Chris Sander

Science, New Series, Vol. 273, No. 5275. (Aug. 2, 1996), pp. 595-602.

Stable URL:

http://links.jstor.org/sici?sici=0036-8075%2819960802%293%3A273%3A5275%3C595%3AMTPU%3E2.0.CO%3B2-I